Proceedings of the ASME 2022
International Mechanical Engineering Congress and Exposition
IMECE2022
October 30–November 3, 2022, Columbus, OH

IMECE2022-94850

A MACHINE LEARNING FRAMEWORK FOR PHYSICS-BASED MULTI-FIDELITY MODELING AND HEALTH MONITORING FOR A COMPOSITE WING

Gaurav Makkar[1]*, Cameron Smith[1], George Drakoulas[2,3], Fotis Kopsaftopoulous[1], Farhan Gandhi[1]

[1]Rensselaer Polytechnic Institute, Troy, NY
[2]FEAC Engineering P.C., Patras, Greece
[3]Department of Mechanical Engineering and Aeronautics, University of Patras, Patras, Greece

ABSTRACT

Computational mechanics is a useful tool in the structural health monitoring community for accurately predicting the mechanical performance of various components. However, high-fidelity models simulated through the finite element analysis (FEA) necessitate a large amount of computing power. This paper presents a new approach to develop a multi-fidelity model using artificial neural networks for health monitoring purposes. The proposed framework provides significant savings in computational time compared to a model trained only using high-fidelity data, while maintaining an acceptable level of accuracy. The analysis is conducted using two finite element models, of different fidelity, of an unmanned aerial vehicle (UAV) wing, with damage modeled at six locations, and varying severity. The damage is modeled by changing the stiffness properties of the materials at these locations. The algorithm developed aims at minimizing the number of high-fidelity data points for correcting the outputs of the low-fidelity model. It was observed that the low-fidelity model requires 8 high-fidelity data points to meet the desired error tolerance. This corrected low-fidelity model is then used for locating and quantifying the damage given the strains and frequency by expanding the previously trained network to output damage diagnosis results. The model with applied correction is able to locate the damage with an accuracy of ∼ 94% and quantify the damage with an accuracy of 93%. The performance of the corrected low-fidelity model is compared with a network trained only with high-fidelity datasets and it was observed that the corrected model requires 54% fewer data points as compared to the high-fidelity trained network.

Keywords: Multi-fidelity modeling, Artificial neural network, Model correction, Finite element analysis, Structural health monitoring

*Corresponding author: makkag@rpi.edu
Documentation for `asmeconf.cls`: Version 1.30, August 1, 2022.

NOMENCLATURE

Roman letters

f	Low-fidelity model
g	High-fidelity model
h	Error function

Superscripts and subscripts

HF	High-fidelity
LF	Low-fidelity

1. INTRODUCTION

Composite materials have been used widely to construct lightweight structures for aerospace applications. In order to improve the reliability, safety, and life cycle of these structures, it is important to integrate structural health monitoring (SHM) technologies, making the life-cycle monitoring more efficient, accurate, and robust. Monitoring using vibration-based methods that utilize changes in modal parameters have been applied for damage detection in some studies [1, 2]. There are some related studies which identify damage location and severity using modal shapes [3, 4] and modal frequencies [5, 6].

Data acquisition is the one of the primary steps for SHM. For a mechanical system, the structure's response could be obtained experimentally with physical models or computationally using finite element models. Due to practical limitations, it is not always possible to gather experimental measurements. In the simulation space, the studies deploy finely meshed models to get an accurate representation of the model, in the absence of a physical structure. Even though there have been significant advances in computing power during the past few years, many applications that involve large scale problems are still computationally impractical to solve. For example, applications for uncertainty quantification require solving the computational model multiple times. Also, to make decisions in real time, the model needs to be solved rapidly. Achieving this with a high-fidelity finite element model is well beyond reach. Therefore, it is necessary to develop multi-fidelity

models that are both fast to solve, and possess simulation accuracy close to the high-fidelity model [7–10].

Multiple finite element model updating techniques have been tested and published. Some studies have used Bayesian updating procedures with finite element (FE) models for reducing the influence of uncertainties in structural parameters and for improving the correlation between two models [11, 12]. Genetic algorithm and simulated annealing methods have also been used for sensitivity analysis for updating the structural parameters[13]. The objective of most of these methods is to minimize an error function between the two sources of data. The effectiveness of these algorithms usually depends on an appropriate numerical model and the optimized algorithm [14, 15]. These methods require significant computational effort in the model updating process, especially when the number of parameters is large and there is a significant discrepancy between the two models. Given the number of variables used for model updating process, these algorithms are usually data-hungry.

Numerous studies that investigate damage detection using FE models have also been published like, sensitivity-based model updating for damage detection is investigated in [16–18]. The issue with this method is it does not work when the damage is extreme. Damage detection based on statistical and probability based methods has been explored by various research groups. Some of these include application of Taguchi-based FE model updating for damage detection [19] ,and Bayesian framework-based damage detection using FE models in various structures like beams, 2D, and 3D frame structures [20].

The goal of this study is to fuse two numerical models with different fidelities to generate a corrected low-fidelity model. In the first part of the study, a multi-fidelity model that uses a neural network, is developed. This model makes use of the high-fidelity data to make corrections to the low-fidelity model. Once the performance of the corrected low-fidelity model is validated, the next part of the study explores the ability of this model to perform damage diagnosis. The corrected low-fidelity model is used to locate the damage and quantify the damage severity, and its accuracy and damage assessment capabilities are compared with a neural network trained only using the high-fidelity datasets.

2. FINITE ELEMENT MODELING

The integration of computational structural mechanics and SHM has proven to be a vital methodology for generating accurate results during the entire life cycle of UAV wings [21]. In the frame of this research, finite element analysis (FEA) is utilized to prepare and solve the numerical models in the integrated environment of Siemens PLM Simcenter 3D [22]. The modal analysis was carried out with Nastran SOL103 real eigenvalue analysis with the scope to determine the natural frequencies and mode shapes of the structure [23]. In chapters 2.2 and 2.3, high-fidelity and low-fidelity models are constructed to simulate the eigenvalue analysis under both healthy states and various combinations of damage modeling.

2.1 Material Definition

Both isotropic and orthotropic materials are defined to model the actual structural behavior of the UAV wing. In particular, woven carbon fiber fabric (WC-FF) is utilized to improve the high strength to weight ratio compared to conventional materials and avoid the delamination of laminated composites [24–26]. In addition, a carbon fiber unidirectional (CF-UD) material is used to strengthen the wing, while decreasing the overall weight, and thus leading to a reduction in the fuel consumption [27]. The material properties are detailed in Table 1. The subscript annotations indicate the major directions, referring to the longitudinal (1) direction of fibers and the long (2) and short (3) transverse direction of fibers, as well.

FIGURE 1: GEOMETRY DESIGN OF THE UAV WING

TABLE 1: MATERIAL PROPERTIES

FEM	HF & LF		HF & LF		HF & LF
Material	WC-FF		CF-UD		Epoxy
Density, $\rho(kg/m^3)$	600		1600		1300
Young Modulus, E(MPa)	E_{11}	65000	E_{11}	80000	3000
	E_{22}	65000	E_{22}	5000	
Shear Modulus, G(MPa)	G_{23}	100	G_{23}	2500	1094
	G_{12}	100	G_{12}	2500	
Poisson's Ratio, ν	ν_{12}	0.35	ν_{12}	0.28	0.37

2.2 High-Fidelity Finite Element Model

Meshing the wing's components, including the upper and lower skin, two spars, and nine ribs, is the key to obtaining accurate results. The finite element model (FEM) consists of a high-quality, fine mesh grid to enhance numerical convergence and good performance. Since the components are thin-wall structures, and the ratio of the thickness to the in-plane dimensions is high, quadrilateral, isoparametric, plane strain elements are utilized. The density of the finite element grid is derived through a mesh convergence study, aiming to observe slight differences in the displacement and stress results. The entire model comprises of approximately 220,000 elements.

Classical laminate theory (CLT) [28] is applied to calculate the structural performance of the skin and the spars that are represented with composite materials. CLT calculates the mid-plane strain and stresses. A stacked sequence of laminates assembled to form a plate defines the two-dimensional composite layups. A local coordinate system is constructed for each finite element that is aligned with the fiber direction. According to the real-life structure, the composite laminate is defined, including the layups, fiber orientation, and thickness of each ply.

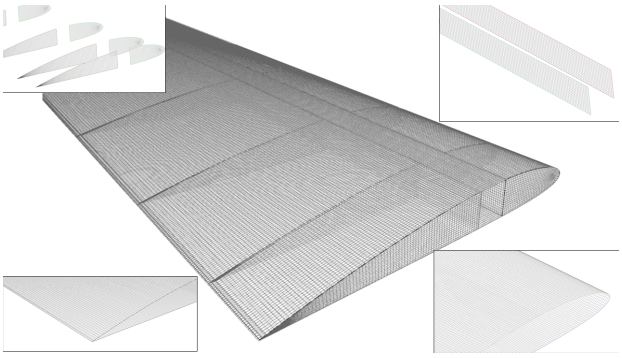

FIGURE 2: MESH GRID OF THE UAV WING

The classical laminate theory states that the 90° orientation of the fibers is employed to sustain the structure from transverse loads and the 0° from the longitudinal [29] loads. The skin distributes the aerodynamic loads throughout the structure while also providing strength against shear and torsional stresses. Therefore, one ply of WC-FF with thickness 0.1 millimeters (mm) is defined to increase the bending stiffness fiber in the 0° and 90° orientations. The spars are made up of four plies with the following layup: [(0,90)/0/0/(0,90)]. The upper and bottom layups are modeled using 0.1mm thick WC-FF plates, while the middle layups are formed with 0.3mm thick CF-UD plates. Ribs are mostly used to maintain the overall aerodynamic shape of the wing, and, thus, isotropic epoxy is utilized with a thickness equal to 0.125mm.

Boundary conditions are necessary to ensure a numerically well-defined problem and to accurately represent real-world phenomena. To establish a relationship between the wing's components and prevent bodies from passing through each other, a bonded contact type is defined for the relevant components. Therefore, the various components share the same nodes at their intersections. The wing is also fixed at the face of the first rib.

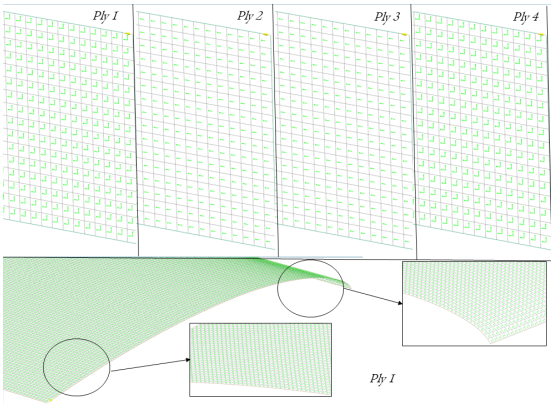

FIGURE 3: MATERIAL ORIENTATION OF THE SPARS(TOP) & SKIN(BOTTOM)

2.3 Low-Fidelity Finite Element Model

After defining the high-fidelity model, a low-fidelity FEM was developed for comparison with the high-fidelity model's simulation data. The model's geometry was adapted directly from that of the high-fidelity model to establish consistency in the models' encompassing dimensions. While both beam element and shell element models were explored for the low-fidelity model, shell elements were ultimately chosen. This decision was made because using shell elements for both models allows for a more direct comparison between the models' simulation data. A visualization of the low-fidelity model is shown in Figure 4.

To construct this low-fidelity model, mesh collectors were created to define the different sections of the model. All of the rib objects, represented in blue in Figure 4, were assigned to the same mesh collector. However, a unique mesh collector was defined for each of the spar objects, represented in red in Figure 4, to ensure proper fiber orientation and definition for the shell element laminates. Two-dimensional mapped meshes of CQUAD4 type were utilized to create the meshes, but the element sizing varied between 5 mm and 4.5 mm for the rib and spar objects, respectively. Utilizing shell elements for the low-fidelity model allowed for the same material properties as the high-fidelity model to be used, which are included in Table 1. Therefore, the isotropic epoxy was assigned to all of the rib objects in the low-fidelity model. Additionally, since damage will ultimately be applied to the skin of the high-fidelity model as discussed in section 2.4, the layup for the skin referenced in 2.2 was used for the spar objects. Finally, the low-fidelity model was fixed along the edge of its first rib to establish consistency between the two models.

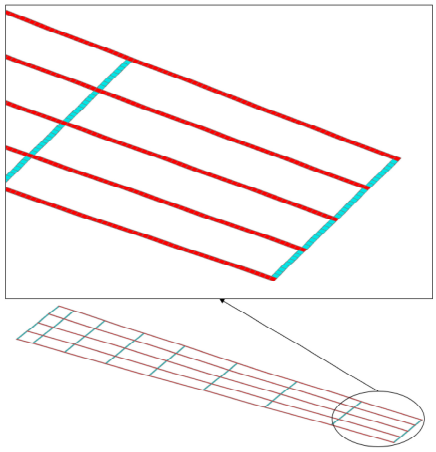

FIGURE 4: LOW-FIDELITY SHELL ELEMENT WING MODEL

2.4 Damage Modeling

Sections 2.2 and 2.3 describe the unaltered, healthy models that are utilized for this study. However, a key component of the machine learning framework outlined in this study is to use the framework for health monitoring. Therefore, both models need to be constructed so that certain regions can simulate structural damage. Despite the inherent differences in the models, damage is simulated in the same manner. First, six damage regions are defined across the wing's structure for all three models, as shown in Figure 5. Within each region, elements are extracted

and sorted into separate mesh collectors that reflect their corresponding damage region. For the low-fidelity model, elements are extracted from the second and fourth spars, while the high-fidelity model elements are only extracted from the top surface of the skin. Although performing mesh extraction retains the definition of the composite layups in both models, adjustments to the materials are necessary to allow for differentiation between the damage regions. In the high-fidelity model, six copies of the WC-FF material are made, and one copy is assigned to each mesh collector, which represent the damage regions A-F. Defining each damage region with independent materials enables easier automation when performing the real eigenvalue analysis. A similar procedure is followed for the low-fidelity model. As mentioned previously in section 2.3, the low-fidelity model's spar objects utilize the high-fidelity model's skin layup outlined in section 2.2. Thus, six copies of the WC-FF material are again created in the low-fidelity model to represent the material properties in the damage regions.

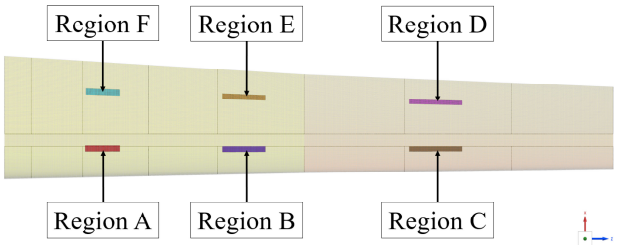

FIGURE 5: WING DAMAGE REGIONS

To model damage within a given region, the regional values for the elastic and shear moduli shown in Table 1 are multiplied by a percentage between 0 and 100. For example, a damage of 25% to the WC-FF signifies that the elastic and shear moduli values are multiplied by 0.75 to reduce the material's stiffness. This allows for localized damage to be modeled in the wing since the material properties can be modified separately by damage region. Four total damage classes are also defined to represent the damage extent or how much the material properties are affected. These classes are defined as 1-25% damage, 26-50% damage, 51-75% damage, and 76-99% damage. To simplify the notation, each damage class is assigned a number from 1 through 4, where lower numbers correspond to a lower damage class. Combining this notation with the damage regions in the wing, the damage location and extent can be defined by two characters: the first alphabetic and the second numeric. For example, "B2" signifies that damage exists in region B and the extent of the damage is somewhere in the range of 26-50%.

After establishing how damage is modeled across the wing, simulation test matrices are generated to be used for the eigenvalue analysis. These test matrices fall into two primary categories regarding their usage for the neural networks: training and validation. For training purposes, 25 predefined combinations are created. One wing with no damage is simulated, and then damage extents of 25, 50, 75, and 99% are applied in each of the regions A-F across the wing. To validate the neural network frameworks, an additional 24 cases are simulated. Instead of using predetermined values for the damage extent for the validation studies, modifiers for the material properties are selected from a normal distribution with a mean of 0.4 and a standard deviation of 0.1. Again, four randomly determined damage extents are simulated in each region. A summary of the simulation cases that are conducted is provided in Table 2. In order to expedite and automate the simulation cases, the Hierarchical Evolutionary Engineering Design System (HEEDS) software developed by Siemens is utilized. The material properties defined in Table 1 are given as the input variables to the evaluation studies, and the first 20 eigenfrequencies and ply strain data on the models' skins are tagged as the response variables of interest.

TABLE 2: SUMMARY OF SIMULATION CASES

Purpose for NN:	Damage Extent Method:	Number of Simulation Cases:
Training	Predetermined	25
Validation	Randomly determined	24

2.5 FEA Results

For both the HIFI and LOFI models, the first 4 eigenfrequencies and mode shapes are presented in the Figure 6 to visualize the torsion and bending in the models.

3. MODEL CORRECTION AND DAMAGE DIAGNOSIS

3.1 Model Correction Algorithm

In the frame of this research paper, the numerical values (e.g. strain fields) used to formulate and validate the machine learning procedure are extracted through modal analysis.Even though these values do not preserve any physical meaning, the objective is to construct a robust data-driven methodology that can be adapted to have physical applications.

As described earlier, there are two finite element models. It is important to ascertain the elements on the high-fidelity model which are located at the same coordinates as elements in the low-fidelity model. The strains are then compared between the low-fidelity model and the new, filtered high-fidelity model. For the present study the high-fidelity model will be referred to as (**g**) and the low-fidelity model will be referred to as (**f**). The low-fidelity model is not accurate, but it can be queried at effectively no time or cost. Conversely, while the high-fidelity model is assumed to have negligible error, it is very expensive in terms of computational time and cost. The low-fidelity model predicts a quantity Y. The predicted value $\hat{Y}$ has an unknown associated error, E. This can be written as

$$\mathbf{f}(u) = \hat{Y} \tag{1}$$

$$\hat{Y} = Y + E \tag{2}$$

$$\mathbf{g}(u) = Y \tag{3}$$

Another way to exploit this relationship between the high-fidelity and low-fidelity models is to make use of correlation that exists

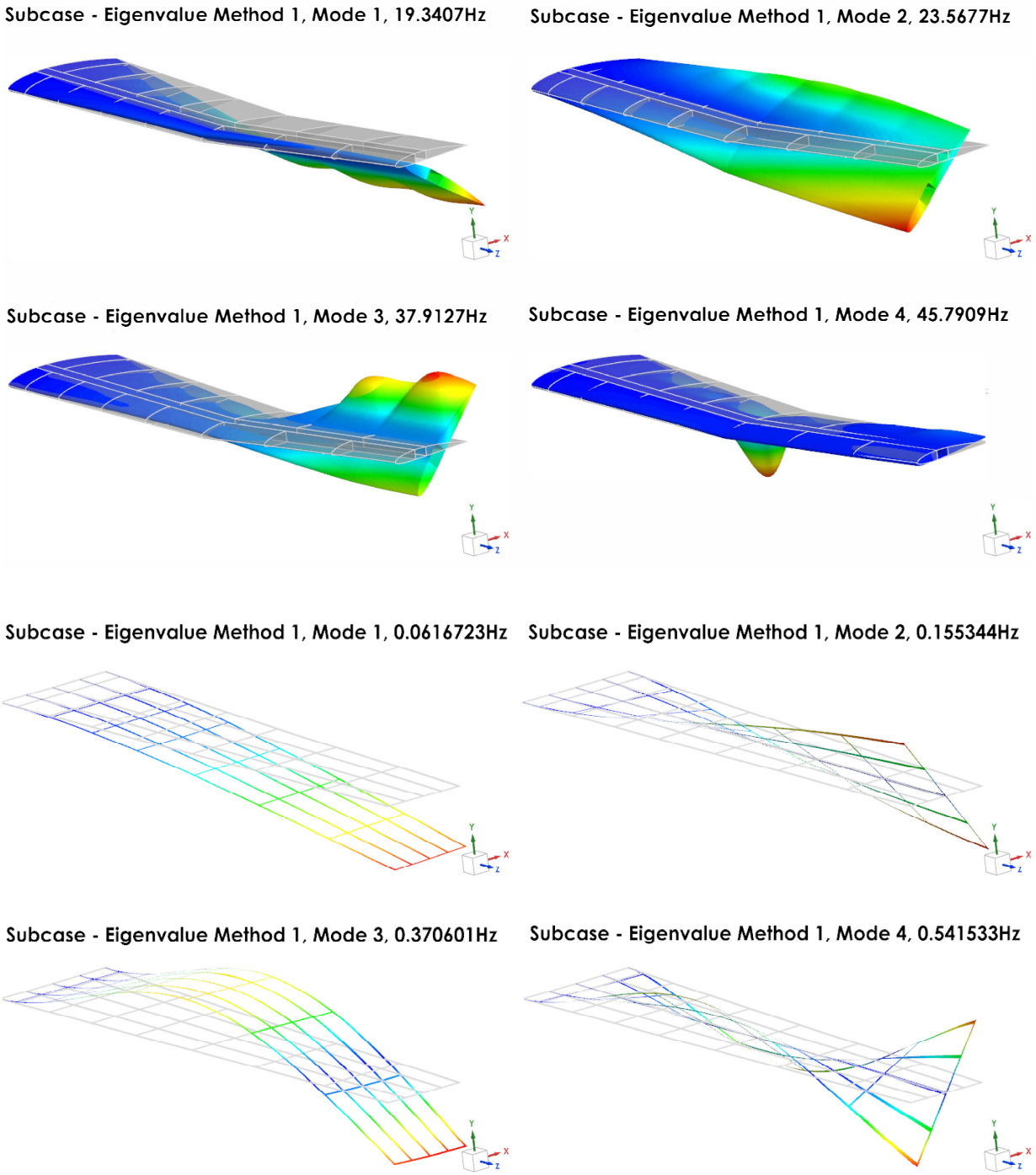

FIGURE 6: HIFI (TOP) & LOFI (BOTTOM) MODAL ANALYSIS RESULTS

between the two models. This can be written as

$$\mathbf{g}(u) = \rho\mathbf{f}(u) + e \tag{4}$$

Here, ρ is responsible for the linear relationship between the two models, and the remaining differences in the two models are captured by the non-linear function e. This is done in order to make the training process less strenuous. Instead of learning the function E (Eq. 2), the neural network needs to learn e. If it is assumed that the error e is due to modeling error, then there exists a function $\mathbf{h}$ which is dependent only on observable quantities.

$$\mathbf{h}(u) = e \tag{5}$$

This study uses artificial neural network (ANN) to determine the estimate of this function $\hat{h}$. Artificial neural networks have been a popular choice for AI and machine learning applications since they are capable of modeling any arbitrary function, which can be proved using the universal approximation theorem. Also,

depending on the non-linearity of the problem, ANN can change the number of neurons in the hidden layer. Neural networks usually fall into one of two categories depending on the type of problem they address: classifiers and regressors. A classifier is a neural network that is trained to categorize some piece of information based on a set of variables which are called predictors. A regressor, on the other hand is trained to make predictions on a continuous domain as a function of predictor variables. For SHM applications, regressor neural networks have been used in health and usage monitoring applications [30, 31]. The nature of the current problem involves modeling continuous variables using a regressor neural network and then quantifying the damage severity by classifying it into one of the categories defined in section 2.2. For the purposes of regression, the artificial neural networks need to use numerically stable neuron activation functions. A rectified linear unit activation function is used for the study presented in this paper.

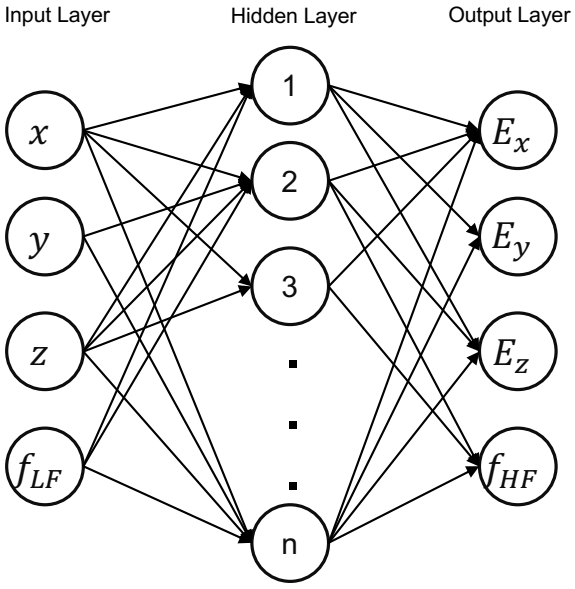

FIGURE 7: NEURAL NETWORK ARCHITECTURE

The back-propagation learning algorithm is the most common approach to tune the weight and bias of a neural network. Levenberg-Marquardt back-propagation is chosen for back-propagation training. The artificial neural network used in the this study consists of a single hidden layer of neurons, with each neuron in the hidden layer connected to every input node and every output node, as shown in Figure 7. The input node consists of the x,y,z coordinates of each node and the frequencies from the low-fidelity model (f_{LF}). The output consists of error in the strain in the three axis at all the nodes and the high-fidelity frequencies (f_{HF}). These inputs are scaled to a range of [-1, 1] before training. The output layer gives the estimated correction as a linear combination of the weighted hidden outputs and bias. The hidden layer size is set to 14 neurons, which minimizes root mean square error (RMSE) as shown in Figure 9 which shows the variation in RMSE with hidden layer size using 1-fold cross validation. The algorithm used for correction is shown in figure 8 and is outlined as follows:

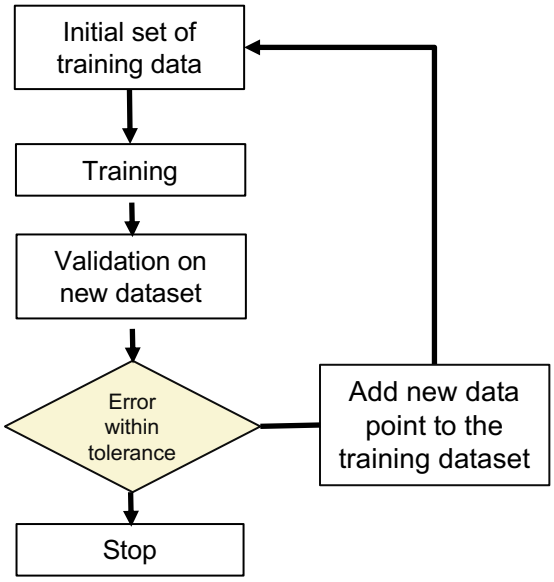

FIGURE 8: LOCALIZATION AND QUANTIFICATION ALGORITHM

1. The training starts with an initial set of data.
2. Once the trained model is available, it is used to make corrections on a new dataset which was not used in the training process.
3. The tolerance on a particular output is defined by the user. For the present study, if the normalized strains obtained after applying corrections to the low fidelity model are within 5% of the true value of strain, given by the high-fidelity model, the training process stops and the algorithm quits. If the corrections are not accurate, the validated dataset is added to the training dataset and the process is carried out again.

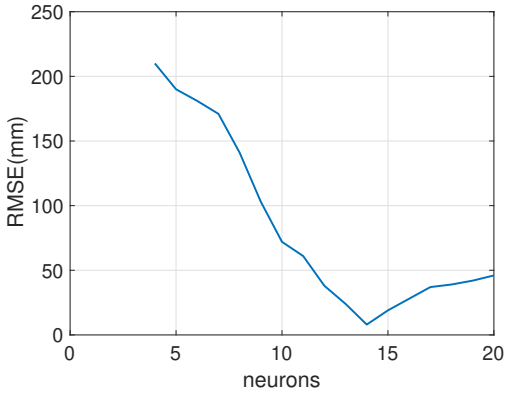

FIGURE 9: 1-FOLD CROSS VALIDATION SHOWING VARIATION IN NEURAL NETWORK POWER CORRECTION MODELING ERROR WITH INCREASED HIDDEN LAYER SIZE

3.2 Damage Diagnosis Algorithm

Once the corrections are made, the corrected low-fidelity model can be used to localize the damage on the wing, given

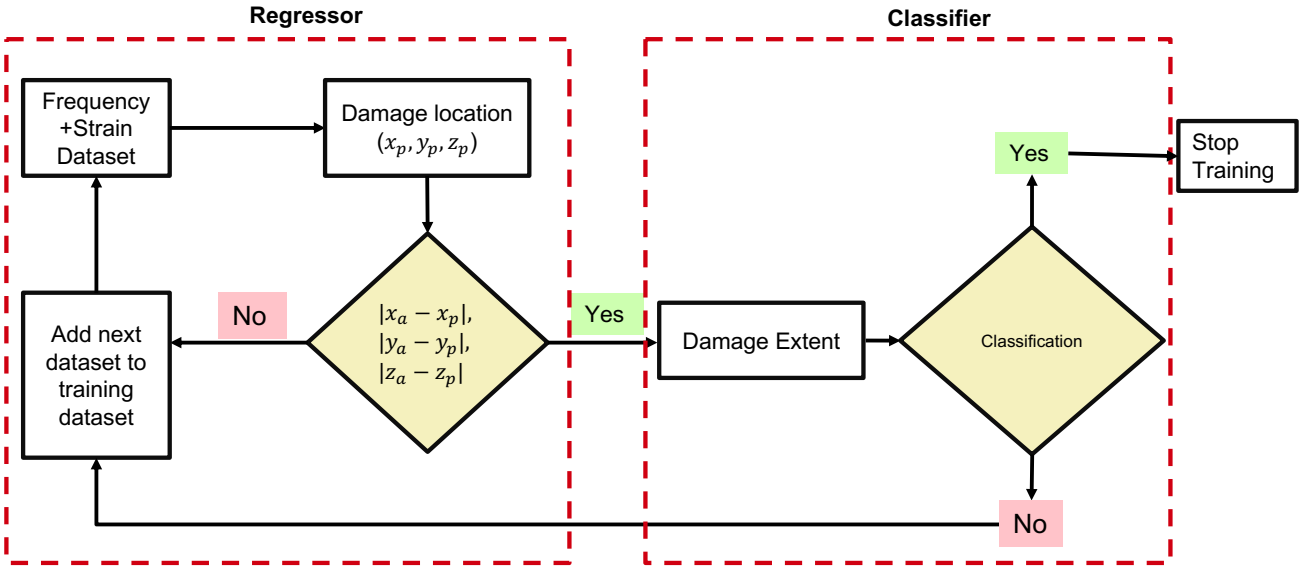

FIGURE 10: LOCALIZATION AND QUANTIFICATION ALGORITHM

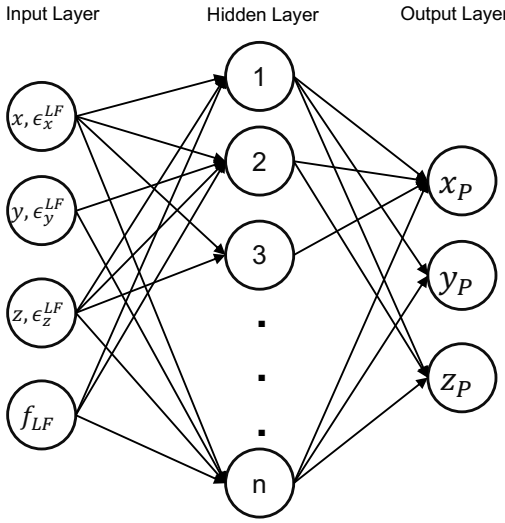

FIGURE 11: NEURAL NETWORK ARCHITECTURE FOR DAMAGE DIAGNOSIS

strain data and natural frequencies. The block diagram of the algorithm for localization of damage is shown in Figure 10.

The algorithm starts with a small training dataset. For the present case, the starting number of the dataset is 3 simulation cases. This dataset is used to train a neural network shown in figure 11. The neural network outputs the x,y, and z coordinates of the centroid of the predicted damage location. When the initial set of data does not produce sufficiently accurate predictions, the model can be improved by selecting new data to evaluate and retrain the corrected model. The following algorithm is used to iteratively select additional data from **g** to add to the training data.

1. For the n^{th} iteration, $\mathbf{f} + \hat{h}_n$ is trained from the available training data and validated with a new dataset.

2. The absolute error between the actual damage location (from **g**) and predicted damage location for the validation data point is calculated.

3. If the absolute error is less than the tolerated error (0.05%), the algorithm moves to quantifying the error. If the error does not meet the tolerance criteria, this tested datapoint is added to the training dataset and the neural network is trained with this enriched dataset.

4. Once the error meets the tolerance criteria, the information from the regressor neural network is passed to the classifier neural network. The classifier makes use of all the existing dataset used from training the regressor neural network. Just like the regressor, a new validation dataset is picked randomly and the trained classifier is used to classify the damage extent. If the classifier categorizes the damage extent correctly, the training stops and the regressor-classifier network is used to make predictions on the testing dataset to evaluate its generalization characteristics.

4. RESULTS

4.1 Model Correction

The strain values are used for comparing the two models and making appropriate corrections. A total of 24 low-fidelity damage cases and 24 high-fidelity damage cases are available across the 6 damage locations along with a healthy dataset for both models. Therefore, for each finite element model, 25 datasets exist. Out of these datasets, 10 are reserved for testing the generalization characteristics of the trained network. Three low-fidelity and high-fidelity datasets are randomly chosen to train a neural network as described in the algorithm section (Section 3.1). The trained model is then validated with a new dataset until the corrected strain values are within 10% of the true strain value obtained from the high-fidelity dataset. The training process requires 8 datasets before it meets the desired tolerance. Once the training process stops, the model is validated on the remaining

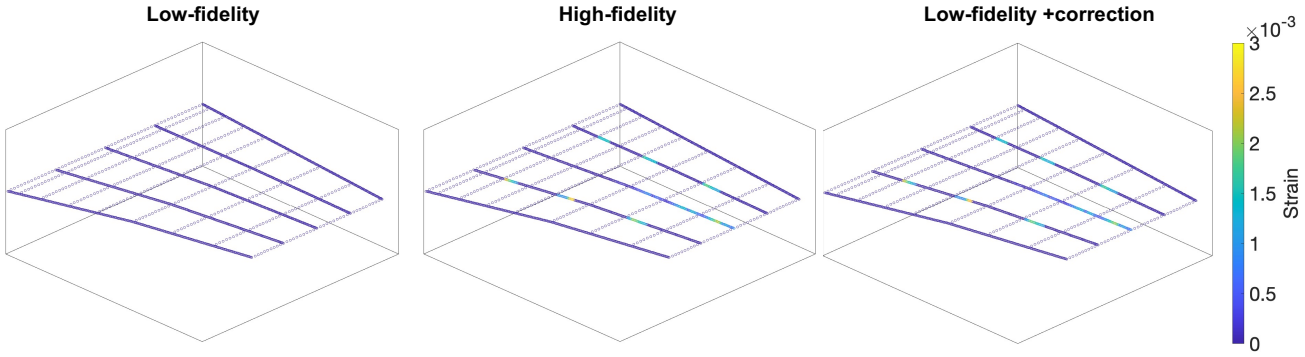

FIGURE 12: STRAIN COMPARISON

dataset. The strains for the low-fidelity, high-fidelity, and corrected model for a single load case are shown in Figure 12. It is evident that the corrected low-fidelity model predicts strain accurately. The summary of performance of the trained network on the testing dataset is given in Table 3. Note that even though only 10 datasets are reserved for testing the generalization characteristics, the training process does not utilize all of the available datasets. Thus, the remaining datasets can also be used for the testing, which totals 17 datasets that are used for testing the accuracy of the corrected model. Table 4 compares the frequency of the low-fidelity, high-fidelity, and corrected models across all the damage cases for the six damage locations for 99% damage. It is clear that the corrected low-fidelity model accurately predicts the modal frequencies.

TABLE 3: SUMMARY OF NEURAL NETWORK CORRECTION

Damage Locations	RMSE (%)
A	5.2
B	7.1
C	7.9
D	9.1
E	6.1
F	5.3

TABLE 4: FREQUENCY OF FIRST MODE WITH 99% DAMAGE

Location	Frequency (Hz) Low-fidelity	Frequency (Hz) High-fidelity	Frequency (Hz) Corrected
A	0.37	19.32	18.2
B	0.39	19.36	18.9
C	0.41	19.37	18.7
D	0.42	19.32	19.5
E	0.34	19.39	18.6
F	0.38	19.34	18.9

4.2 Damage Diagnosis - Corrected Low-Fidelity Model

The algorithm for localization of damage and classification, or quantification, is discussed in section 3.2. The corrected model obtained in section 4.1 is used for this study. The model correction process used 8 high-fidelity datasets. This acts as the starting model for the algorithm. The problem is an inverse problem, where the objective is to find the location of the damage given the strains and frequency. Therefore, the inverse of the corrected model is used for the training (Figure 11). The inputs to this neural network are the coordinates, x, y, and z, and the respective strains from the low-fidelity model, ϵ_x^{LF},ϵ_y^{LF}, and ϵ_z^{LF}, at those coordinates. All the input nodes are attached to all the neurons in the hidden layer. The output from this is the predicted damage location coordinates.

After each training iteration the predicted damage location is compared with the actual damage location given by the high-fidelity dataset. For the present study, the tolerance is 5% of the span. This means if the predicted coordinates (x_P,y_P, and z_P) are within 5% of actual (x_a,y_a, and z_a) damage locations, the trained model meets the required tolerance and no more points are added in the training dataset for localization. If the accuracy is not within the allowable tolerance, this new dataset is added to the training set, and the process is repeated for a new randomly chosen dataset.

Once the learning method achieves desired accuracy in locating the damage, the algorithm moves to the next step, which is classifying the damage in one of the four categories of damage (i) 0% - 25%, (ii) 26% - 50%, (iii) 51% - 75%, and (iv) 76% - 99%. These percentages refer to the reduction in the stiffness at the damage locations.

For quantification, the training for the neural network starts with the latest training dataset. The trained classifier is used to make a prediction on the damage extent for a new, incoming dataset. The quitting criteria for the classifier is correct classification of the incoming dataset.

Figure 13 shows the results for the localization and quantification with increasing the number of datasets. Since 8 datasets were used for correcting the low-fidelity model, the process starts with 8 datasets (grey area in the plot). With 8 datasets, a neural network is trained and validated on a new dataset to output the location of the damage. The RMSE as fraction of the total span of the wing is more than the allowable tolerance of 5% (orange-dashed line). Hence, this dataset is added to the training dataset, and the process is repeated. With this enriched training dataset, the new network prediction meets the tolerance criteria. At this point with 9 datasets used in the training, the regressor neural network stops (yellow-dashed line).

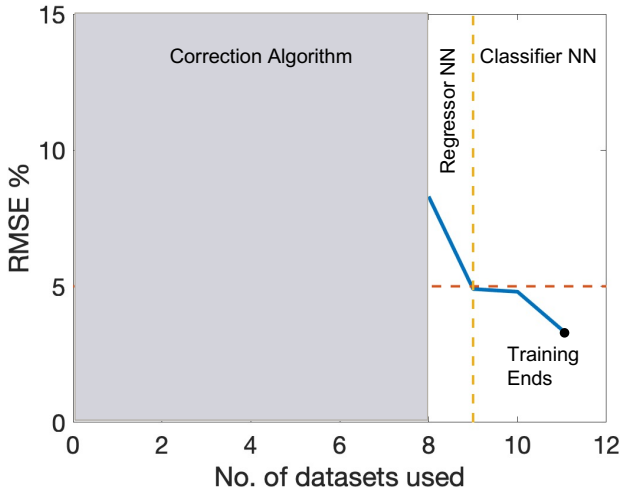

FIGURE 13: CONVERGENCE FOR DAMAGE DIAGNOSIS - CORRECTED LOW-FIDELITY MODEL

Once the desired confidence has been established on the regressor neural network, the next step is accurate classification. The classifier starts with nine datasets. These are the datasets that have already been used for the localization process. Thus, there is no additional computational cost associated here. Once the classifier has been trained, it is used for validation on a new dataset. The classifier assigns the dataset to one of the four damage classes discussed in section 2.4. If this categorization is correct, the training ends, otherwise the dataset is added to the training set, and the weights of the neural network are trained again. In Figure 13, it is shown that for classification, the training process required 2 more datasets. Thus, the total number of datasets required for this entire training process was 11. At this point training concludes.

To analyze the trained network, the performance is evaluated on a test dataset. This dataset has damage simulated at the same locations, but the extent of damage is randomly distributed as discussed previously in section 2.4. A total of 24 datasets were tested, and the summary is given in table 5. It is evident that for the testing dataset with normally distributed damage, the trained network is able to locate the damage with 93% accuracy and classify it into the correct damage class 22 out of 24 times.

TABLE 5: DAMAGE DIAGNOSIS RESULTS - CORRECTED MODEL

Dataset	RMSE (%)	Quantification Accuracy (%)
Validation	5.7	100
Testing	6.3	91.6

4.3 Damage Diagnosis - High Fidelity Model

To test the value of low-fidelity model for improving predictive capabilities with sparse data, a purely data-driven model based only on the high-fidelity dataset is used for comparison. The idea behind this model is to find the relationship between the system variables without any explicit knowledge of the underlying process.

TABLE 6: NUMBER OF DATASETS USED

Dataset	Corrected Low-Fidelity Model	High-Fidelity Model
Training	11	24
Testing	24	24

The difference in the approach for training in this section is absence of a low-fidelity model to make corrections. The machine learning model now makes predictions on the high-fidelity data instead of predictions with a corrected low-fidelity model. The process remains similar. When the corrected low-fidelity model was being used, the training started with 8 datasets. In this case, since there is no prior training for correction, the algorithm can be initialized from a small number. For this study, the training begins with 3 datasets. The inputs are the strains and frequencies from the high-fidelity model, and the output is the location of the damage. The algorithm keeps on adding datasets for training until the RMSE for the incoming dataset meets the tolerance criteria. Once the regressor network is trained, the algorithm moves to classifying the damage into one of the four categories.

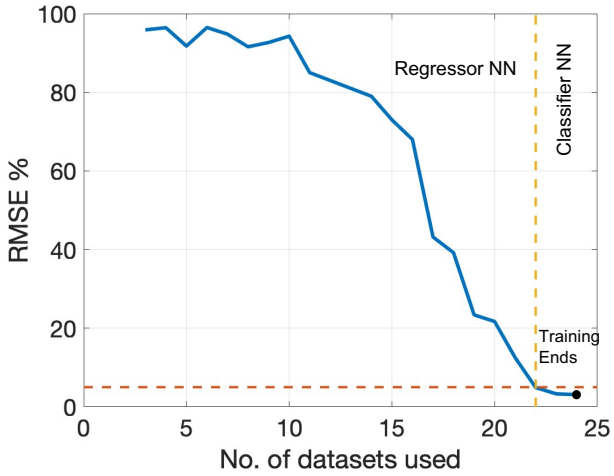

FIGURE 14: CONVERGENCE FOR DAMAGE DIAGNOSIS ALGORITHM- HIGH FIDELITY MODEL

TABLE 7: DAMAGE DIAGNOSIS RESULT - HIGH-FIDELITY MODEL

Dataset	RMSE (%)	Quantification Accuracy(%)
Validation	3.8	100
Testing	4.8	95.8

Figure 14 shows the performance of the learning method with increasing number of datasets when it uses only the high-fidelity datasets. Even though it is possible to reach the desired tolerance, the major deficiency in this approach is the additional data required. Table 6 summarizes the number of datasets used for training and testing. Compared to the network trained with corrected model, which required 11 total datasets, the network trained using only the high-fidelity model uses 24 datasets. Therefore, it requires 13 additional high-fidelity datasets to achieve the

same level of accuracy. This result confirms the substantial effect that the low-fidelity model has in reducing data dependency. This may be attributed to the neural network being provided with a reasonable initial guess that can be expanded upon with further training. Table 7 provides a summary of the performance criteria of the trained network on the same testing dataset. The accuracy of predicting the damage location is only 2.3% higher than the corrected model. The network trained only on the high-fidelity model makes the correct classification 23 out of 24 times.

5. CONCLUSIONS

This study evaluates the ability of artificial neural networks to correct the low-fidelity estimates of frequency and strains observed for a UAV wing. The estimates are corrected using a high-fidelity model. This corrected model is then used for localization and classification of damage. An algorithm that enriches the training dataset based on a predefined tolerance is developed. The algorithm takes in data randomly from the available datasets to check the generalization properties of the trained network.

The analysis confirms that it is possible to make appropriate corrections to the low-fidelity model with a small number of high-fidelity datasets, and the accuracy is improved to 97%. Additionally, the study also establishes the capability of a corrected model to localize the damage and classify it into one of the specified damage categories. The trained model was able to locate the damage correctly with an accuracy of 93.7% and classify it correctly 93% of the times.

Finally, the study makes a comparison to a data-driven model based only on the high-fidelity dataset in order to identify and evaluate the contribution of the low-fidelity model. The corrected model required almost 54% less datasets as compared to the model trained solely on high-fidelity dataset to achieve similar accuracy. Future steps include the application of the developed approach in various cases in the field of computational mechanics such as, static and/or transient structural analysis.

REFERENCES

[1] Montalvao, Diogo, Maia, Nuno Manuel Mendes and Ribeiro, António Manuel Relógio. "A review of vibration-based structural health monitoring with special emphasis on composite materials." *Shock and vibration digest* Vol. 38 No. 4 (2006): pp. 295–324.

[2] Carden, E Peter and Fanning, Paul. "Vibration based condition monitoring: a review." *Structural health monitoring* Vol. 3 No. 4 (2004): pp. 355–377.

[3] Douka, E, Loutridis, S and Trochidis, A. "Crack identification in beams using wavelet analysis." *International Journal of solids and structures* Vol. 40 No. 13-14 (2003): pp. 3557–3569.

[4] Zhu, XQ and Law, SS. "Wavelet-based crack identification of bridge beam from operational deflection time history." *International Journal of Solids and Structures* Vol. 43 No. 7-8 (2006): pp. 2299–2317.

[5] Patil, DP and Maiti, SK. "Detection of multiple cracks using frequency measurements." *Engineering Fracture Mechanics* Vol. 70 No. 12 (2003): pp. 1553–1572.

[6] Ye, Junjie, He, Yumin, Chen, Xuefeng, Zhai, Zhi, Wang, Youming and He, Zhengjia. "Pipe crack identification based on finite element method of second generation wavelets." *Mechanical Systems and Signal Processing* Vol. 24 No. 2 (2010): pp. 379–393.

[7] Forrester, Alexander IJ, Sóbester, András and Keane, Andy J. "Multi-fidelity optimization via surrogate modelling." *Proceedings of the royal society a: mathematical, physical and engineering sciences* Vol. 463 No. 2088 (2007): pp. 3251–3269.

[8] Pinti, Orazio, Niemiec, Robert, Oberai, Assad A and Gandhi, Farhan. "A Multi-Fidelity Approach to Predicting Rotor Aerodynamic Interactions." *AIAA AVIATION 2020 FORUM*: p. 2796. 2020.

[9] Robinson, TD, Eldred, Michael S, Willcox, Karen E and Haimes, Robert. "Surrogate-based optimization using multifidelity models with variable parameterization and corrected space mapping." *AIAA journal* Vol. 46 No. 11 (2008): pp. 2814–2822.

[10] Makkar, Gaurav, Reddinger, Jean-Paul, Gandhi, Farhan and Kopsaftopoulos, Fotis. "Machine Learning Based Approach to Improve Low-Fidelity Predictions for a Compound Helicopter." *Proceedings of the 77th Vertical Flight Society Annual Forum, Virtual, May 10–14* .

[11] Simoen, Ellen, Papadimitriou, Costas and Lombaert, Geert. "On prediction error correlation in Bayesian model updating." *Journal of Sound and Vibration* Vol. 332 No. 18 (2013): pp. 4136–4152.

[12] Goller, B and Schueller, GI. "Investigation of model uncertainties in Bayesian structural model updating." *Journal of sound and vibration* Vol. 330 No. 25 (2011): pp. 6122–6136.

[13] Levin, RI and Lieven, NAJ. "Dynamic finite element model updating using simulated annealing and genetic algorithms." *Mechanical systems and signal processing* Vol. 12 No. 1 (1998): pp. 91–120.

[14] Zhang, QW, Chang, Tse-Yung Paul and Chang, Chih Chen. "Finite-element model updating for the Kap Shui Mun cable-stayed bridge." *Journal of Bridge Engineering* Vol. 6 No. 4 (2001): pp. 285–293.

[15] Jaishi, Bijaya and Ren, Wei-Xin. "Structural finite element model updating using ambient vibration test results." *Journal of structural engineering* Vol. 131 No. 4 (2005): pp. 617–628.

[16] Fritzen, C-P, Jennewein, D and Kiefer, Th. "Damage detection based on model updating methods." *Mechanical systems and signal processing* Vol. 12 No. 1 (1998): pp. 163–186.

[17] Zheng, ZD, Lu, ZR, Chen, WH and Liu, JK. "Structural damage identification based on power spectral density sensitivity analysis of dynamic responses." *Computers & Structures* Vol. 146 (2015): pp. 176–184.

[18] Mordini, Andrea, Savov, Konstantin and Wenzel, Helmut. "Damage detection on stay cables using an open source-based framework for finite element model updating." *Structural Health Monitoring* Vol. 7 No. 2 (2008): pp. 91–102.

[19] Sun, Hang and Liu, Yang. "An improved Taguchi method and its application in finite element model updating of bridges." *Key Engineering Materials*, Vol. 456: pp. 51–65. 2011. Trans Tech Publ.

[20] Behmanesh, Iman and Moaveni, Babak. "Probabilistic identification of simulated damage on the Dowling Hall footbridge through Bayesian finite element model updating." *Structural Control and Health Monitoring* Vol. 22 No. 3 (2015): pp. 463–483.

[21] Kosmatka, John and Oliver, Jesse. "Development of an in-flight structural health monitoring system for composite unmanned aircraft." *47th AIAA/ASME/ASCE/AHS/ASC Structures, Structural Dynamics, and Materials Conference 14th AIAA/ASME/AHS Adaptive Structures Conference 7th*: p. 1881. 2006.

[22] "SIEMENS PLM Simcenter 3D." URL www.plm.automation.siemens.com.

[23] "SIEMENS Simcenter 3D: Basic dynamic analysis user's guide." URL https://docs.plm.automation.siemens.com/data_services/resources/nxnastran/10/help/en_US/tdocExt/pdf/basic_dynamics.pdf.

[24] Misra, RK, Dixit, Anurag and Mali, Harlal Singh. "Finite element (FE) shear modeling of woven fabric textile composite." *Procedia materials science* Vol. 6 (2014): pp. 1344–1350.

[25] Grodzki, W and Łukaszewicz, A. "Design and manufacture of umanned aerial vehicles (uav) wing structure using composite materials: Planung und bau einer flügelstruktur für unbemannte luftfahrzeuge (uav) unter verwendung von kompositwerkstoffen." *Materialwissenschaft und Werkstofftechnik* Vol. 46 No. 3 (2015): pp. 269–278.

[26] Basri, Ernnie Illyani, Sultan, Mohamed Thariq Hameed, Basri, Adi Azriff, Mustapha, Faizal and Ahmad, Kamarul Arifin. "Consideration of Lamination Structural Analysis in a Multi-Layered Composite and Failure Analysis on Wing Design Application." *Materials* Vol. 14 No. 13 (2021): p. 3705.

[27] Holmes, Mark. "Aerospace looks to composites for solutions." *Reinforced Plastics* Vol. 61 No. 4 (2017): pp. 237–241.

[28] Raju, Ivatury S and Wang, John T. "Classical laminate theory models for woven fabric composites." *Journal of Composites, Technology and Research* Vol. 16 No. 4 (1994): pp. 289–303.

[29] Campbell, Flake C. *Structural composite materials*. ASM international (2010).

[30] Shen, Ting, Wan, Fangyi, Song, Bifeng and Wu, Yun. "Damage location and identification of the wing structure with Probabilistic Neural Networks." *2011 Prognostics and System Health Managment Confernece*: pp. 1–6. 2011. DOI 10.1109/PHM.2011.5939524.

[31] Papatheou, Evangelos, Manson, Graeme, Barthorpe, Robert J and Worden, Keith. "The use of pseudo-faults for damage location in SHM: An experimental investigation on a Piper Tomahawk aircraft wing." *Journal of Sound and Vibration* Vol. 333 No. 3 (2014): pp. 971–990.

[32] Hertel, Lars, Collado, Julian, Sadowski, Peter, Ott, Jordan and Baldi, Pierre. "Sherpa: Robust hyperparameter optimization for machine learning." *SoftwareX* Vol. 12 (2020): p. 100591.

[33] Irving, Philip E and Soutis, Costas. *Polymer composites in the aerospace industry*. Woodhead Publishing (2019).